

Designing unconventional Fmoc-peptide-based biomaterials: structure and related properties

Cite this: *Soft Matter*, 2014, 10, 1944

Laura Chronopoulou,^a Simona Sennato,^b Federico Bordi,^b Domenico Giannella,^a Antonio Di Nitto,^a Andrea Barbetta,^a Mariella Dentini,^a Anna Rita Togna,^c Giuseppina Ines Togna,^c Sabina Moschini^c and Cleofe Palocci^{*a}

We have recently employed L-amino acids in the lipase-catalyzed biofabrication of a class of self-assembling Fmoc-peptides that form 3-dimensional nanofiber scaffolds. Here we report that using D-amino acids, the homochiral self-assembling peptide Fmoc-D-Phe₃ (Fmoc-F*F*F*) also forms a 3-dimensional nanofiber scaffold that is substantially distinguishable from its L-peptide and heterochiral peptide (F*FF and FF*F*) counterparts on the basis of their physico-chemical properties. Such chiral peptides self-assemble into ordered nanofibers with well defined fibrillar motifs. Circular dichroism and atomic force microscopy have been employed to study in depth such fibrillar peptide structures. Dexamethasone release kinetics from PLGA and CS-PLGA nanoparticles entrapped within the peptidic hydrogel matrix encourage its use for applications in drug controlled release.

Received 18th September 2013
Accepted 16th December 2013

DOI: 10.1039/c3sm52457d

www.rsc.org/softmatter

Introduction

As it is well known, enzymatic reactions have become increasingly attractive tools for the fabrication of advanced materials¹ and aECM (artificial extracellular matrix) engineering.² Most enzymes catalyze chemical reactions at low temperatures, neutral pH and in buffered aqueous solutions, mild conditions under which many conventional chemical reactions fail. Enzymes can also be exceptionally selective towards their substrates, allowing for sophisticated, biologically inspired aECM design, without the complication of side-reactions and cellular toxicity.^{3,4}

Indeed, recent development efforts in this area have produced a number of remarkable examples for such smart enzyme responsive materials.¹

In particular, much effort has been focused on the study of various self-assembling peptides and their relevance in biology, protein aggregation and nanobiotechnological applications.⁵⁻⁹ Not surprisingly, most of this work has been carried out using naturally occurring L-form amino acids. It has been reported that some peptides undergo conformational changes in the presence of external stimuli such as temperature, pH, ionic strength and metal ion binding manipulations.¹⁰⁻¹⁵ Certain peptides were found to exhibit remarkable secondary structure

plasticity and multifaceted behavior, including the ability to undergo secondary structural transitions directly from β-sheet to α-helix in response to changes in temperature or pH.¹⁶ In each of these cases, the studied peptides were composed of L-form amino acids. Subsequently numerous self-assembling peptides with various compositions, sequences, and lengths have been studied largely by using peptides composed of L-amino acids.^{5-11,17,18} However, although there was a nagging question about their chiral counterparts, no detailed attempt has been made to study their mirror image forms, namely, self-assembling peptides made of only D amino acids, until recently.

Since D-form peptide bonds are more resistant to enzyme degradation than their enantiomeric L-form, D-peptide based materials will likely be more stable *in vivo*. Thus, a new class of D-form self-assembling peptides may prove to be very versatile in fabricating novel supramolecular architectures and have a wide range of applications in biotechnology, nanobiotechnology and medical technology.

Some authors¹⁹ have recently investigated in detail a class of self-assembling peptides by studying a chiral mirror image peptide, d-EAK16, which is made of only D-amino acids of alternating hydrophilic and hydrophobic residues. Moreover, the same authors have carried out systematic studies on the d-EAK16 peptide, evidencing the formation of interesting stable secondary structures.²⁰ The rheological studies and agglutinating activity examination showed that there were significant differences between all D-amino acid-peptide d-EAK16, and mixed D,L-amino acid peptides EA*K16 and E*AK*16.

In the past we reported the rapid Fmoc-L-Phe₃ self-assembling peptide biosynthesis in aqueous phase and the ability of using such peptide hydrogel as a scaffold for culturing rat microglial cells.^{21,22}

^aDepartment of Chemistry, Sapienza University of Rome, Piazzale Aldo Moro 5, Rome 00185, Italy. E-mail: cleofe.palocci@uniroma1.it; Fax: +39 06 490324; Tel: +39 06 49913317

^bDepartment of Physics and CNR-IPCF, Sapienza University of Rome, Piazzale Aldo Moro 5, Rome 00185, Italy

^cDepartment of Physiology and Pharmacology "Vittorio Ersparmer", Sapienza University of Rome, Via degli Apuli 4, Rome 00185, Italy

Here we report some recent results on the lipase-catalyzed formation of self-assembling Fmoc-Phe₃ peptides made of all D-amino acids or alternating DLL and LDD amino acids. In addition to the formation of nanofibers the D-form and mixed D,L-peptides were able to self-organize into 3D nanofiber scaffolds, like their L-counterpart.²² The peptides can form a β -sheet-like molecular structure with D-chirality to give the mirror image of the circular dichroism (CD) spectrum of its L-peptide counterpart. Also we entrapped a model drug within the hydrogel matrix and we studied its release kinetics in an aqueous medium.

Materials and methods

Materials

Fluorenylmethoxycarbonyl-L-phenylalanine (Fmoc-F) (>99%), fluorenylmethoxycarbonyl-D-phenylalanine (Fmoc-F*) (>99%), L-diphenylalanine (FF) (>99%) and D-diphenylalanine (F*F*) (>99%) were purchased from Bachem GmbH (Weil am Rhein, Germany). Lipase from *Pseudomonas fluorescens* (PFL) was kindly provided by Amano Enzyme Inc. (Nagoya, Japan).

All other chemicals were purchased from Sigma Aldrich (St. Louis, Missouri) and used without further purification. All solvents used in HPLC analysis were of HPLC grade and used as received.

Biosynthesis of peptide hydrogels

Fmoc-tripeptide hydrogels were prepared following previously published procedures.²¹ Briefly, 40 μ mol of each substrate, an Fmoc-amino acid and a dipeptide, were suspended in a mixture of 1 ml of H₂O and 420 μ l of 0.5 M NaOH until obtaining a homogeneous dispersion. Then, 0.1 M HCl was added to reach a final pH value of 7, with a final volume of 3 ml. A fixed amount (100 μ l) of lipase solution (50 mg ml⁻¹) was added to the substrate suspension and the mixture was placed in a thermostated bath at 30 °C. All experiments were performed at least in triplicate.

The lipase-catalyzed gelation of Fmoc-triphenylalanine tripeptides (Fmoc-Phe₃) was studied for reaction times up to 40 min. Tripeptide final reaction yields were calculated indirectly by measuring Fmoc-amino acid disappearance in the reaction medium by HPLC analysis, as previously described by the authors.²¹

Swelling studies

In order to obtain information on the physical structure of the synthesized hydrogels, we measured the swelling ratio of each sample.

The swelling ratios of F-moc hydrogels with the same initial total concentration were measured using PBS. All the Fmoc peptide based hydrogels were weighed after their preparation (W_i). Then 3 ml of PBS (pH 7.4) were added to each hydrogel, which were then placed in an incubator at 30 °C overnight. Fully swollen hydrogels were weighed (W_s) immediately after the removal of excess water. Then, the hydrogels were freeze-dried and weighed (W_d). The swelling behavior was expressed as the

swelling ratio q , which is the ratio of the weight of the swollen sample (W_s) and the weight of the freeze-dried hydrogel (W_d) ($q = (W_s - W_d)/W_d$) or as percentage of weight loss ($W_l = (W_i - W_s)/W_i$ %). Each experiment was performed in triplicate.

Circular dichroism spectroscopy

Circular dichroism measurements on samples with 0.02 wt% or 0.2 wt% peptide concentrations were performed at room temperature (30 °C) on a Jasco J-815 spectropolarimeter. Samples at 3.7×10^{-5} M and pH 10 (adjusted with NaOH when necessary) were placed in a quartz cuvette with a path length of 1 cm. Spectra were recorded between 300 and 200 nm with a step size of 0.2 nm. Data were truncated below the wavelength at which the HT reading indicated that there was not enough light incident on the detector. The bandwidth was set to 1 nm with a scanning speed of 50 nm min⁻¹ and a digital integration time of 2 s. In order to improve the signal to noise ratio, nine spectra were recorded and averaged. Millidegrees of rotation were converted to molar residual ellipticity.

Dynamic rheological measurements

The time for the onset of gelation and the evolution of elasticity was determined by rheometry in a constant strain mode. The measurements were performed with a Bohlin CS10 (version 4.033) operating in the oscillatory mode, with an imposed amplitude of deformation of 1% and a frequency of 1 Hz, both monitored using a stress-controlled rheometer. The value of the strain amplitude was checked to ensure that all measurements were performed in the linear-viscoelastic regime, where the dynamic storage modulus (G') and loss modulus (G'') are independent of strain amplitude. Coaxial cylinder geometry (C10) was used for the analysis of 3 ml samples. The sample cuvette of the rheometer was closed with a tightly fitted, hollowed Teflon disk in order to prevent solvent evaporation. The rheometer was equipped with a temperature control unit that was calibrated to give a known, constant temperature in the sample chamber. The elapsed time between mixing/injection and start of the data collection was approximately 60 s for all experiments. The gelation process was followed at 30 °C.

Here, we report the storage moduli of the samples during the gelation process. Each experiment was repeated at least three times to obtain the mean and standard deviation.

Storage and loss moduli of the formed gels were determined as a function of the applied frequency in the range 0.01–10 Hz at 25 °C.

AFM measurements

AFM images of the peptidic hydrogels were acquired in air at room temperature using a Dimension Icon (Bruker AXS) instrument. Considering that in the imaging of soft biopolymers with AFM at high resolution it is important to minimize the tip tapping force, we employed the Scan Asyst™ mode. This imaging mode allows the application of lower forces than standard tapping mode by using an algorithm operating in Peak Force Tapping™, which continuously monitors the quality of the image and self-optimizes the acquisition

parameters. During a measurement employing Scan Asyst™, a very fast force–separation curve is obtained at every pixel in the image and the peak force is used by the feedback signal. In this way it is possible to use a precisely controlled force at each pixel, thus allowing the application of lower imaging forces than standard tapping mode, protecting soft samples from damage without compromising the image resolution. We used dedicated probes characterized using an ultra-sharp silicon tip (nominal radius of curvature 2 nm) mounted on a triangular silicon nitride cantilever, with a very low spring constant (0.4 N m^{-1}) and a nominal resonant frequency of 70 kHz, allowing for the required high level force control on soft samples in air.

Sample preparation for AFM measurements was performed according to this protocol. Aliquots of 10–20 μl were removed from the peptide hydrogel suspension at the end of the gelation process and deposited onto the freshly cleaved mica surface. To optimize the amount of peptide adsorbed, each aliquot was left on mica for 5 minutes and then gently washed with 200 μl of Milli-Q water. The mica surface with the adsorbed peptide was then flushed with a stream of nitrogen for drying, and analyzed after 30 min. Images analyzed using the NanoScope Analysis software v 1.40 (Bruker) and the Gwiddion free software are presented as raw data, except for flattening. No further image processing was carried out. For the statistical estimation of average values of the height of the fibers and of the pitches for each sample, 50 total counts have been analyzed using the Nanoscope Analysis software. Pitches have been determined considering the distance between the maxima of the longitudinal profiles. The results reported in the table represent the mean and the statistical uncertainties of the mean.

Cell cultures

All the employed procedures were in accordance with European Communities Council Directive no. 86/609/EEC.

Microglial cells were obtained from the cerebral cortex of 1- or 2-day old decapitated rats as previously described.²³ Briefly, the cortices were dissected and digested in 0.125% trypsin and in the presence of 50 kU ml^{-1} of Dnase I. Cells were plated at a density of 4.5×10^4 cells per cm^2 in T75 flasks in 10 ml medium D-MEM, supplemented with 10% FCS and antibiotics (100 IU ml^{-1} of penicillin and 100 $\mu\text{g ml}^{-1}$ of streptomycin).

The medium was changed within 24 h, and then twice a week. After 10–14 days from dissection, microglia were detached from the astrocyte monolayer by shaking, and the cells were re-suspended in DMEM/F12 medium (10% FCS and antibiotics).

The cells were then placed in 24-well plastic plates at a density of 4×10^5 cells per ml, incubated at 37°C in a humidified atmosphere containing 5% CO_2 and allowed to adhere. The purity of microglial cell populations (>98%) was verified by staining with IBA-1 (1 : 1000) antibody. After 2 h the medium was replaced with 1 ml of fresh medium.

Microglial cells were treated with F*F*F*, FFF, F*FF or FF*F*Fmoc tripeptide solution (0.3, 3, 30 and 100 $\mu\text{g ml}^{-1}$) for 24 h.

Assessment of cell viability/proliferation

The MTT (3-(4,5-dimethylthiazol-2yl)-2,5-diphenyltetrazolium bromide) reduction assay was used to assess cell viability/proliferation.^{24,25} After an incubation time of 24 h with the peptides, media were discarded; cells were washed and incubated for 4 h at 37°C with MTT (0.5 mg ml^{-1} final concentration).

The supernatant was removed and the pellet washed with isotonic phosphate-buffered saline (PBS: 0.137 M NaCl, 3 mM KCl, 1.9 mM NaH_2PO_4 , 8.1 mM Na_2HPO_4 , pH 7.4). Finally, addition of 100 μl of dimethyl sulfoxide was needed to dissolve the blue formazan product (reduced MTT), which was quantified by measuring the absorbance at 570 nm test wavelength.

Dexamethasone *in vitro* release experiments

Dexamethasone-loaded hydrogels at 0.1% (w/v) nanoparticle concentration were prepared by adding PLGA and PLGA CS-coated nanoparticles entrapping dexamethasone, or the corresponding amount of free dexamethasone, during Fmoc-F*F*F* formation. Briefly, the precursor solutions were prepared by mixing 1.36 mg of dexamethasone or 3 mg of PLGA nanoparticles, prepared as described in previous work,²⁶ and gel forming components (see peptide biosynthesis), and poured into a 5 ml Pyrex vial before gelation. The mixture was then incubated at 30°C for 2 h for gelation. A release medium, 2 ml PBS pH 7.4, was then added to each vial, and the vial was placed in a thermostated bath at 37°C . The whole release medium was replaced to maintain an infinite sink condition at each time point. The amount of released dexamethasone at each time point was analyzed by HPLC, equipped with a UV detector set at 243 nm.

Results and discussion

Lipase-catalyzed hydrogel biosynthesis

Both Fmoc-F and Fmoc-F* were used in lipase-catalyzed reversed hydrolysis reactions using respectively F*F* and FF dipeptides, with the formation of a peptide bond between an Fmoc-aminoacid and a dipeptide. The reaction conditions for such bioconversion have been optimized in a previous work.²¹ Fig. 1a shows the kinetic profiles of PFL-catalyzed Fmoc-FFF, Fmoc-F*F*F*, Fmoc-FF*F* and Fmoc-F*FF formation. All the studied bioconversions afforded a self-supporting hydrogel in the employed reaction conditions in about 20 minutes, as evidenced by the inversion test (Fig. 1b and c).

The initial reaction rate for Fmoc-FFF formation appears to be higher than that for its chiral counterpart Fmoc-F*F*F*, as expected since the active site of the enzyme has a stronger affinity towards substrates with L-chirality. Fmoc-FFF synthesis occurs with a reaction yield of approximately 30%. On the other hand, even if the initial reaction rate for Fmoc-F*F*F* formation is lower, the conversion in this case reaches approximately 50%. Probably, in this case, the low reaction rate allows the enzyme to remain in the solution phase for a longer time and work at a higher local concentration of the substrate. Moreover, we must keep in mind that a dynamic equilibrium is present,

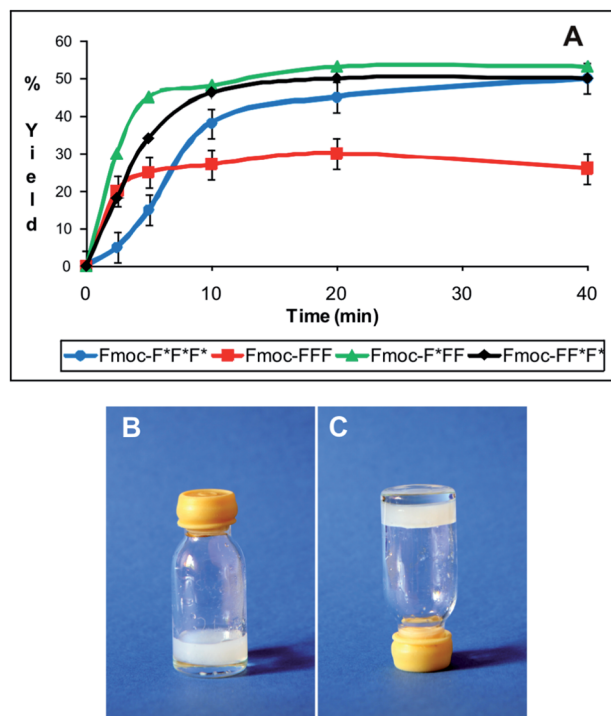


Fig. 1 (a): Fmoc-FFF (red), Fmoc-F*F*F* (blue), Fmoc-F*FF (green) and Fmoc-FF*F* (black) formation kinetics catalyzed by PFL. Reaction conditions: 40 μ mol of Fmoc-aminoacid and dipeptide, 5mg of lipase, aqueous phase volume 3 ml, pH 7.0, $t = 30$ $^{\circ}$ C. (b and c) Inversion test of a hydrogel sample.

where the biocatalyst can also hydrolyze the reaction product. Since PFL has a stronger affinity for substrates of ι -chirality, the hydrolysis of the reaction product is most likely higher for Fmoc-FFF than for Fmoc-F*F*F*, contributing to the difference in the formation yields obtained for the two peptides.

As far as the synthesis of the peptides with mixed chirality is concerned, the initial reaction rate is higher for Fmoc-FF*F* than Fmoc-F*FF. Taking into account that the substrate that is bound by the enzyme in its active site forming the acyl-enzyme intermediate is the Fmoc-peptide, such finding correlates with PFL stronger affinity towards the substrate with natural chirality, Fmoc-F. The kinetic profiles of the two reactions both reach a similar plateau value in about 20 minutes, corresponding to a conversion of approximately 50%.

Rheological characterization

Time sweep experiments on the solutions of Fmoc-F*F*F* and Fmoc-FFF (Fig. 2a) at a single frequency provide information about the rate and extent of the gelling process. In both cases the cross-over point between G' and G'' traces which marks the gelation time could not be observed. Already at ~ 1 min, the time at which the first point was recorded, $G' > G''$ indicating that the system has turned into a predominantly solid-like system. From Fig. 2 it can be clearly seen that the evolution of the storage modulus with time is quite different for the four systems under analysis. In the case of Fmoc-F*F*F*, the G' trace increased with curing time and leveled off reaching a plateau

value of 3.5 kPa after approximately 12 h. The initial rise in the modulus follows the establishment of a three-dimensional network structure, and involves the conversion of an increasing amount of units in the sol fraction into gel: the subsequent slower rise in the modulus would be caused by further cross-linking paralleled by annealing processes such as rearrangement of crosslinks and lateral chain aggregates. Fmoc-FFF showed a different behavior. G' reached a maximum value of 2.9 kPa at a much faster rate than Fmoc-F*F*F* (less than 1 h), then G' decreased at a slower rate. After 10 h, the solid modulus showed a dramatic reduction (90% of the initial value), pointing out the low tolerance of the gel matrix to the external shear force which was in agreement with the easy disruption and liquid leakage of the transient gels observed during their manipulation. The mixed chirality peptide Fmoc-FF*F* showed a steep rise in G' reaching the highest value recorded among the four peptides, but the curve exhibited abrupt decreases, indicating gel breakdown during network development. In fact, G' increased further, reaching a value of almost 6 kPa after 5.6 h. From this point on, G' underwent a sudden drop in value followed by a rapid decrease. This phenomenon can be ascribed to syneresis. Water is expelled out of the matrix and this may cause the bob to slip on the gel surface, which translates into an abrupt decrease of G' . From this point on, data must be considered to be invalidated by the heterogeneity of the system. Analogous slipping phenomena occurring as the result of syneresis have been observed elsewhere for other polymers.²⁷ Fmoc-F*FF displayed an intermediate behavior between those of Fmoc-FFF and Fmoc-FF*F*. After reaching a maximum at 1.5 h the modulus underwent a moderate decrease followed by a plateau and slow decrease. The peculiar behavior of Fmoc-FF*F*, in particular the first sudden drop in modulus, might be ascribed to the fast gelation kinetics which probably do not allow the developing network to reach a stable configuration, giving rise under stress to a local breakdown of the network.

The frequency spectra of Fmoc-F*F*F*, Fmoc-FFF and Fmoc-F*FF (the latter were determined, respectively, in correspondence of the maximum and of the first plateau after approximately 5 h) point out the formation of stable materials (Fig. 2b). The $\log G'(\omega)$ and $G''(\omega)$ profiles show very small dependences on the angular frequency within the range from 0.1 to 10 rad s^{-1} . This is consistent with the build-up of solid-like hydrogel networks for both gelling pairs. Moduli referring to Fmoc-F*F*F* are about 23% higher than those referring to Fmoc-FFF.

CD results

The CD spectra of Fmoc-F*F*F* and Fmoc-FFF (Fig. 3a) are exactly mirror-like showing bands at 220, 230 and 260 nm. This observed Cotton effect in the amide absorption region (210–220 nm) is presumably due to the π - π^* transitions of the amide bond. These transitions are extremely sensitive to coupling with neighboring amide groups.²⁸ The peptides possess two different kinds of aromatic moieties (one belonging to phenylalanine and the other to F-moc groups) and this increases the complexity of the spectra. The shape of the spectra is not ascribable to a specific conformation but has features of

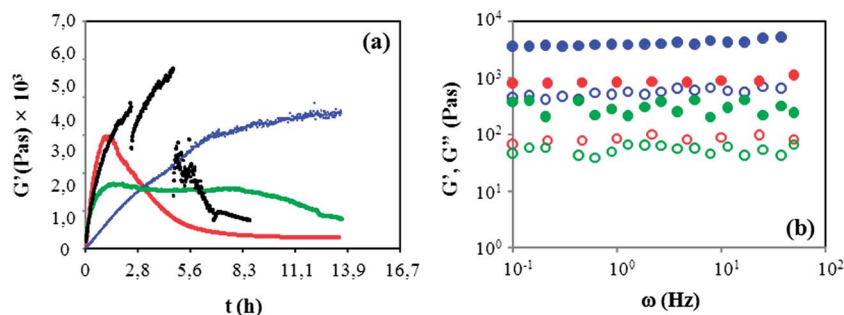


Fig. 2 (a) Storage modulus (G') evolution during isothermal (30 °C) gelation of Fmoc-F*F*F* (blue), Fmoc-FFF (red), Fmoc-F*FF (green) and Fmoc-FF*F* (black). (b) Oscillatory frequency dependence of the viscoelastic moduli of Fmoc-F*F*F*, Fmoc-FFF and Fmoc-F*FF. Full symbol G' , empty symbol G'' .

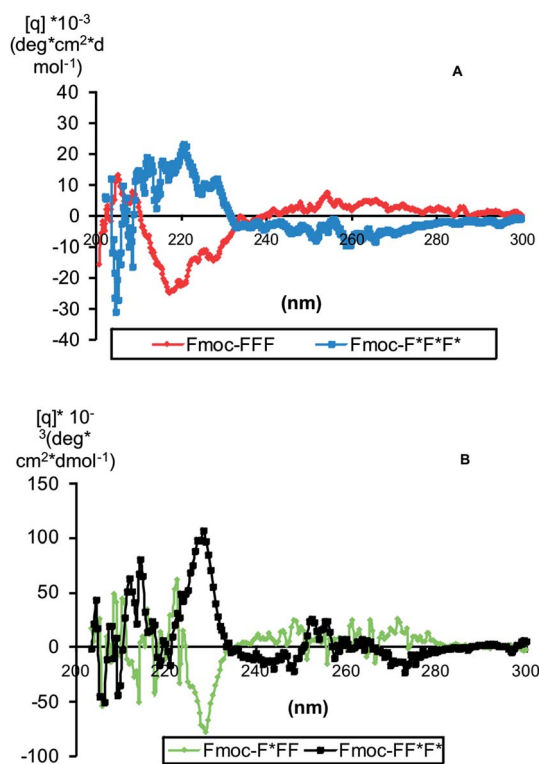


Fig. 3 CD spectra of (a) Fmoc-FFF (red) and Fmoc-F*F*F* (blue) and (b) Fmoc-F*FF (green) and Fmoc-FF*F* (black).

both β -sheet and α -helix. Data gathered from atomic force microscopy (see the AFM results section) provide experimental evidence that peptides stack into the helical supramolecular structure. It is likely that the aromatic groups of different peptides stack up together and interact laterally through hydrogen bonding giving rise to structures reminding β -sheets.

One peculiar feature of the spectra referring to peptides of mixed chirality (Fig. 3b) is the unusually high absorbance of the peak centered at 260 nm, which is remarkably higher than what is usually recorded for protein and peptide solutions [$\sim(10 \div 30) \times 10^3 \text{ deg cm}^2 \text{ dmol}^{-1}$]. This is a symptom of strong aggregation. The solutions of these peptides were turbid and the effect of dilution on absorbance was negligible confirming the presence of aggregates in solution. This hypothesis is in

agreement with the well-known role of aromatic stacking in the formation of chemical and biochemical supramolecular structures.^{29–31}

In conclusion in all the cases examined, the restricted geometry and the attractive forces of the aromatic moieties provide order and directionality as well as the energetic contribution needed for the formation of well-ordered structures.

Swelling determination

Since the swelling behavior of a hydrogel designed for biomedical applications is an important index of its interaction capability with the aqueous based environment in the biological site of application, swelling studies on Fmoc-FFF, Fmoc-F*F*F*, Fmoc-F*FF and Fmoc-FF*F* peptides were also performed. In particular the swelling data relative to the four chiral Fmoc peptides were obtained after incubation of hydrogels in a large amount of PBS (pH 7.4) at 30 °C for 24 h. The results thus obtained, expressed as the ratio (g) or $W_1\%$, are shown in Fig. 4. From the reported data, it is clear that all the hydrogels present very similar and high values of swelling ratios. This behavior takes into account the low peptide concentration within the hydrogel ($\approx 7 \text{ mM}$), independent of peptide chiral composition, in comparison with the overall water content. Conversely, the evaluation of $W_1\%$ upon hydrogel equilibration with PBS seems to be more effective. In fact, as reported in Fig. 4 this parameter

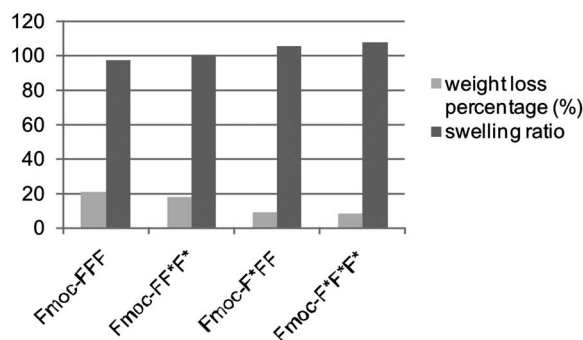


Fig. 4 Weight loss percentage and swelling ratio of Fmoc-FFF, Fmoc-F*F*F*, Fmoc-F*FF and Fmoc-FF*F* peptides.

reflects different gelling behavior of Fmoc-FFF and Fmoc-FF*F* on one side and Fmoc-F*F*F* and Fmoc-F*FF on the other. As also evidenced from rheological measurements, the Fmoc-FFF and Fmoc-FF*F* based hydrogels are less stable and lose 20% of water; the other ones (Fmoc-F*F*F* and Fmoc-F*FF) afforded stronger materials less prone to lose water.

Dexamethasone release studies from peptide hydrogels

It is well known that the mechanical properties of hydrogels are very important for pharmaceutical applications. For example, the integrity of the drug delivery device during the lifetime of the application is very important to obtain FDA approval, unless the device is designed as a biodegradable system.³²

Changing hydrogel chemical composition has been used as a strategy to achieve the desired mechanical properties of a hydrogel. As above mentioned, changing the chiral composition of peptidic hydrogel systems will most likely result in a stronger yet elastic hydrogel. The Fmoc peptide hydrogels with a F*F*F* chiral configuration have been tested as drug delivery matrices. Such hydrogels were chosen because their mechanical properties were the most promising among the materials studied in this work. Fig. 5 shows dexamethasone release kinetics from the peptidic hydrogel matrix as well as from PLGA and CS-PLGA nanoparticles entrapped in the gel. A higher release rate was evidenced for uncoated PLGA nanoparticles in comparison with CS-coated ones. However, both formulations afforded a significantly slow and sustained dexamethasone release over time. This interesting behavior is mostly ascribable to the presence of the hydrogel matrix, since previous studies on the nanoparticles alone evidenced that dexamethasone is entirely released from such formulations within a couple of hours.²⁶

In contrast, free DXM release kinetics from the gel follows a controlled release profile up to 168 h. We suggest that both the gel and PLGA based NPs are able to interact with DXM in a different way and afford its release in a sustained way. PLGA hydrophobicity gives rise to a more stable physical interaction with DXM, providing a plateau after 72 h with a lower total amount of released DXM (15%). The kinetic curve of free DXM,

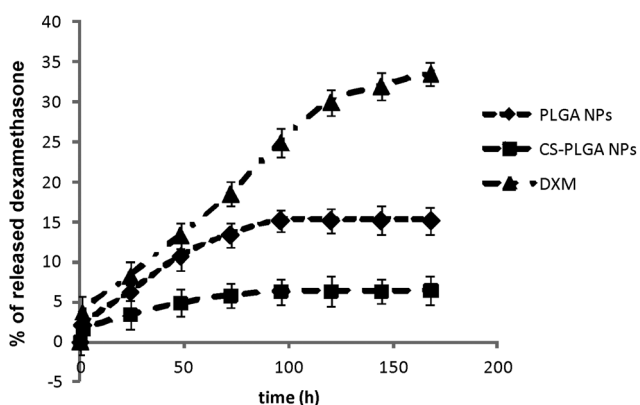


Fig. 5 Dexamethasone release kinetics from the Fmoc-F*F*F* hydrogel matrix, PLGA and CS-PLGA nanoparticles entrapped within the gel.

in contrast, shows a constant drug release even after 72 h with 35% of total DXM released after 168 h. This behavior may be explained on the basis of the higher hydrogel polarity compared to PLGA that shifts toward the NP concentration equilibrium. In this way the direct encapsulation of DXM into the gel seems to provide a more efficient and sustained release over time. However the slower DXM release provided from NPs could be of interest for tissue engineering applications.

Cell studies

In vitro cell compatibility of Fmoc-FFF peptides with D or mixed (DLL or LDD) chirality was evaluated using rat microglia cells and compared with previous results.

As shown in Fig. 6, it appears evident that the microglia cell viability is not negatively influenced by all four Fmoc peptides. In fact, all tripeptides, at concentrations ranging from 0.3 to 30 $\mu\text{g ml}^{-1}$, induce a significant increase in the absorbance value, thus indicating that there are either more cells (perhaps by an increase of adhesion cells) or they are metabolizing the MTT at a higher rate.

AFM studies

Atomic Force Microscopy (AFM) was employed for the investigation of the morphology of fibers and hydrogels.

Fig. 7 shows the height images of the four hydrogels investigated. AFM examinations revealed that all the peptides self-assemble into a network of interconnected nanofibers with lengths of several hundreds of nm and sizes on the order of 8–10 nm.

The Fmoc-FFF tripeptide (Fig. 7A) forms a sparse network with fibers of rather uniform morphology, sometimes interconnected with knots. Fibers appear isolated or very close to each other, but with well distinct borders, which indicates that no fusion or bundle formation occurs.

AFM analysis of the size of Fmoc-FFF fibers gives a narrow size distribution, with a size, measured in the vertical direction of AFM images, of 7.3 ± 0.2 nm. From a closer look at the fibers, the distinctive feature of periodically curved edges which is indicative of a coiled structure is immediately apparent. The *l*-chirality (handedness) of the helix is well visible also at low magnification, in the frame with a lateral size of around 1 micron shown in Fig. 7E, in most of the fibers (see, for example, the fiber marked by the arrow in panel A). Notably, the left-handedness of the helix remains throughout the entire length of the fibers, unperturbed for several hundreds of nm. At higher magnification (Fig. 7 panels E–H) the pitch of the helix can be measured with high accuracy, considering the very low level of noise in the *z*-axis which can be generally obtained with AFM instrumentation (nominally lower than some tenth of Å) and, in particular, Scan Asyst imaging mode (see the Materials and methods section). As reported in Table 1, the pitch of *l*-coiled Fmoc-FFF fibers is estimated to be 17.4 ± 0.1 nm. This value is obtained as the mean value of the peak-to-peak distance measured on the longitudinal height profile, considering several different fibers on the same image, with a minimum of 30 sampling.

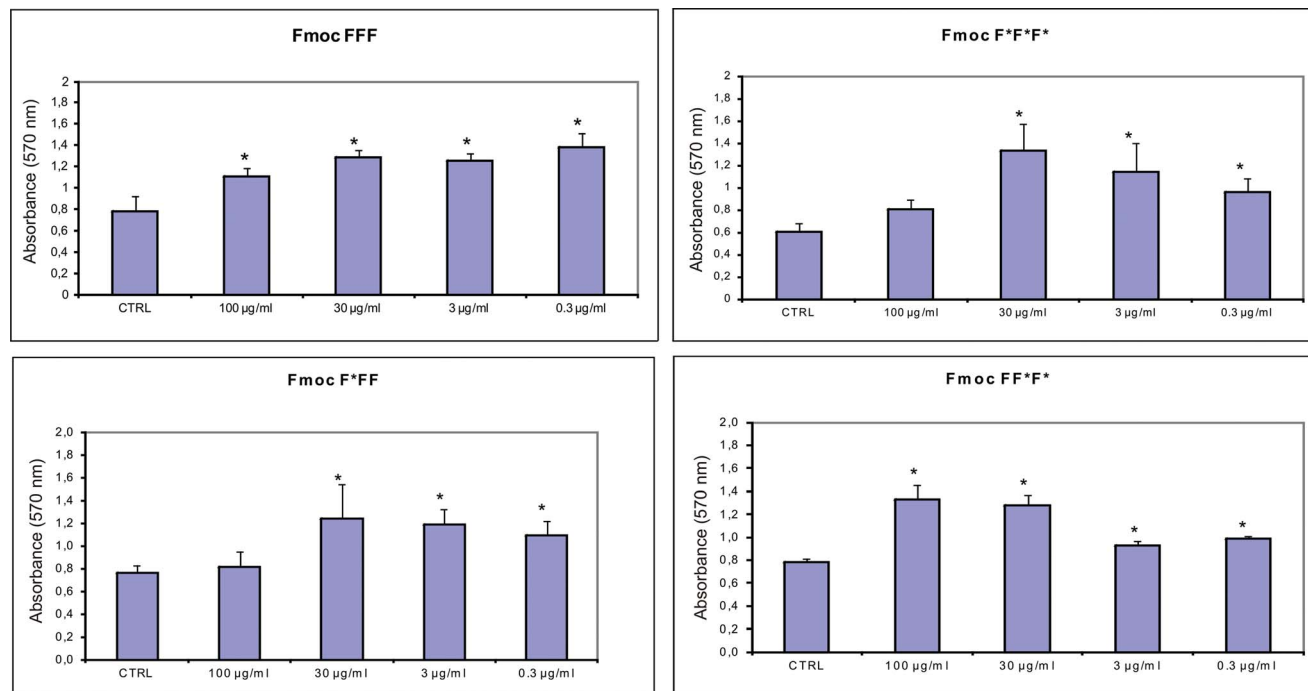


Fig. 6 MTT assays of microglia cells treated with Fmoc-FFF, Fmoc-F*F*F*, Fmoc-F*FF and Fmoc-FF*F* at concentrations between $0.3 \mu\text{g ml}^{-1}$ and $100 \mu\text{g ml}^{-1}$. Values are the means \pm s.d. of six different experiments. Significantly different from control (ctrl): * $p < 0.05$ (one way ANOVA followed by *post hoc* Dunnett's test).

We observed that the peptide composed of all D-amino acids is able to self-assemble into a network with a complex structure of interconnected nanofibers that also form larger bundles

(Fig. 7B). Fmoc-F*F*F* fibers are similar to their L-peptide counterparts for their uniform size, determined to be 7.8 nm from the vertical height profile, but are well distinct for their

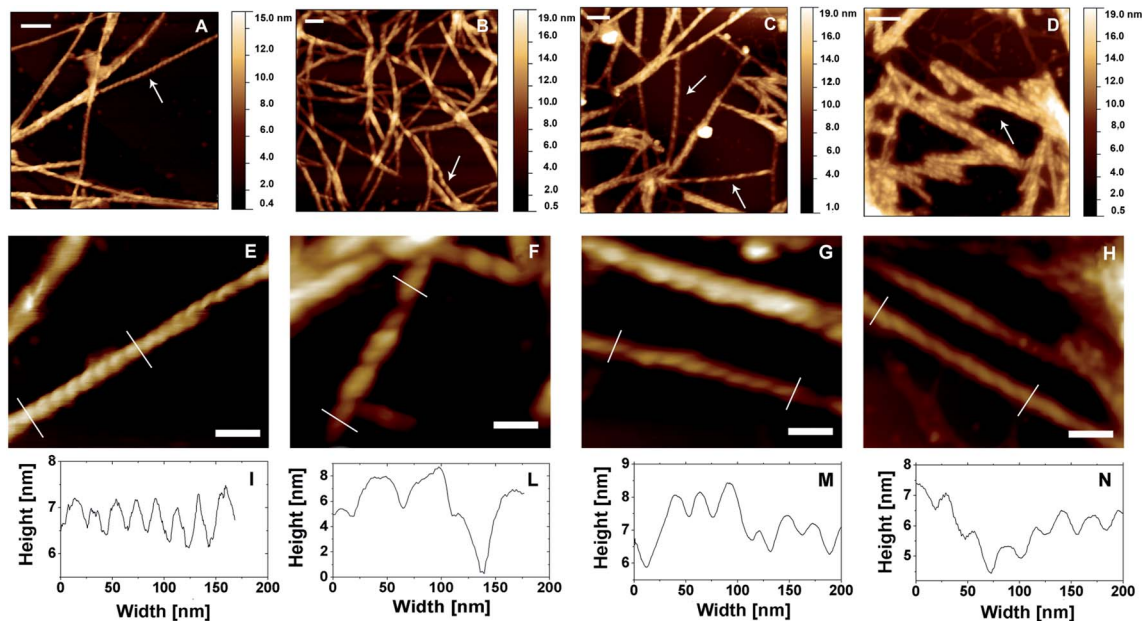


Fig. 7 (A–D) AFM height images of Fmoc-FFF (A), Fmoc-F*F*F* (B), Fmoc-FF*F* (C) and Fmoc-F*FF (D) samples. Arrows indicate fibers where twisting is clearly visible. Bars $\frac{1}{4}$ 100 nm. (E–H) AFM height images of the twisted structure of single nanofibers of Fmoc-FFF (E), Fmoc-F*F*F* (F), Fmoc-FF*F* (G) and Fmoc-F*FF (H) samples. Lines across the fibers mark the portion where the longitudinal section, reported in the corresponding lower panel, has been determined. Bars $\frac{1}{4}$ 50 nm. (I–N) Longitudinal section of single nanofibers of Fmoc-FFF (I), Fmoc-F*F*F* (L), Fmoc-FF*F* (M) and Fmoc-F*FF (N) samples.

Table 1 Structural properties of Fmoc-FFF fibers obtained from analysis of AFM images, for different hydrogels investigated. Values are obtained as the mean value and error is the standard deviation of the mean

Hydrogel chirality	Fiber handedness	Pitch [nm]	Height [nm]
FFF	R	17.4 ± 0.1	7.3 ± 0.2
F*F*F*	L	39.9 ± 2.5	7.8 ± 0.5
FF*F*	R	28.5 ± 1.5	8.1 ± 0.3
F*FF	L	23.5 ± 1	10.1 ± 0.5

opposite coiling. A clearly visible R-handed twist repeats along all the fiber length, and it is found for all the fibers shown in the AFM image, although with different clarity probably due to a variation of the imaging quality during the AFM scan. The pitches are estimated in the order of 39.9 ± 2.5 , significantly larger than the one of Fmoc-FFF. The enlargement of the twisting is accompanied by an increase of the lateral size of the fibers.

According to AFM data the fiber pitch measured for L and D fibers seems to be substantially different (17 and 49 nm respectively). It is interesting to note that fibers having higher pitch values show higher viscoelastic properties than those with lower ones (see Fig. 2). Although the macroscopic properties of such materials reflect the microscopic ones, any kind of speculation on these results should be validated by experimental models able to support the observed physico-chemical properties, in which we are interested for future studies.

On the several AFM images obtained on Fmoc-FFF and Fmoc-F*F*F*, among which the ones reported in panels A and B of Fig. 7 represent the more significant, for these two samples, comparing images with the same area, a lower number of fibers for Fmoc-FFF hydrogels is always observed. Also the number of interconnections and knots between different fibers, as well as the superposition and multiple coiling of fibers, appears to increase, thus contributing to a more entangled organization of the hydrogel scaffold. Nevertheless these observations regarding the complex organization of the hydrogel network should be supported by a more detailed investigation and by a statistical analysis, which is out from the scope of the present work, considering that the samples for AFM imaging have been prepared by using the same protocol, this evident difference between the two hydrogels may be a consequence of different formation kinetics for the two peptides, with higher yield for Fmoc-F*F*F*.

AFM images of mixed Fmoc-FF*F* and Fmoc-F*FF hydrogels are shown in Fig. 7, panels C and D, G and H respectively. The formed networks have an appearance similar to the one of Fmoc-F*F*F*, with numerous interconnected fibers of R and L handedness, for Fmoc-FF*F* and Fmoc-F*FF, respectively.

As shown in Table 1, the pitch of the helix of heterochiral peptides is 28.5 nm and 23.5 nm for Fmoc-FF*F* and Fmoc-F*FF, respectively. Such values may reflect similar mechanical properties. Also the measured height of the fibers is similar for the two peptides, being 8.1 ± 0.3 nm for Fmoc-FF*F* and 10.1 ± 0.5 nm for Fmoc-F*FF. In our opinion fiber formation could be performed in a hierarchical manner: β -sheet-like

peptides form a protofibril, the protofibrils assemble to form a fiber, then fibers coil in a left or right handed fashion to make up a larger fiber, and the helical ribbons further bundle and form a network towards a gel matrix.

In conclusion, our study suggests that the amino acid chirality of self-assembling peptides could be a useful and versatile tool to induce the formation of specific secondary structural features as well as to modulate hydrogel physico-chemical properties.

Conclusions

Our studies provide insight into the importance of chirality for both structure and physico-chemical properties of peptide hydrogels. Moreover, we highlight the possibility of designing specific biomaterials by modulating the composition of their amino acid and related configuration. Since Fmoc-F*F*F* peptides form self-assembled hydrogels that could be also able to resist protease degradation, they could be useful for *in vivo* sustained drug release applications, or as promising bio-materials for a variety of scaffolding applications in soft tissue engineering.

Notes and references

- 1 R. V. Ulijn, *J. Mater. Chem.*, 2006, **16**, 2217–2225.
- 2 D. J. Menzies, A. Cameron, T. Munro, E. Wolvetang, L. Groendahl and J. J. Cooper-White, *Biomacromolecules*, 2013, **14**, 413–423.
- 3 K. M. Park, Y. Lee, J. Y. Son, J. W. Bae and K. D. Park, *Bioconjugate Chem.*, 2012, **23**, 2042–2050.
- 4 L. S. Wang, C. Du, J. E. Chung and M. Kurisawa, *Acta Biomater.*, 2012, **8**, 1826–1837.
- 5 S. Zhang, T. Holmes, C. Lockshin and A. Rich, *Proc. Natl. Acad. Sci. U. S. A.*, 1993, **90**, 3334–3338.
- 6 S. Zhang, C. Lockshin, R. Cook and A. Rich, *Biopolymers*, 1994, **34**, 663–672.
- 7 S. Zhang, T. Holmes, M. DiPersio, R. O. Hynes, X. Su and A. Rich, *Biomaterials*, 1995, **16**, 1385–1393.
- 8 S. Zhang and M. Altman, *React. Funct. Polym.*, 1999, **41**, 91–102.
- 9 T. C. Holmes, S. de Lacalle, X. Su, G. Liu, A. Rich and S. Zhang, *Proc. Natl. Acad. Sci. U. S. A.*, 2000, **97**, 6728–6733.
- 10 S. Zhang and A. Rich, *Proc. Natl. Acad. Sci. U. S. A.*, 1997, **94**, 23–28.
- 11 M. Altman, P. Lee, A. Rich and S. Zhang, *Protein Sci.*, 2000, **9**, 1095–1105.
- 12 B. Ciani, E. G. Hutchinson, R. B. Sessions and D. N. Woolfson, *J. Biol. Chem.*, 2002, **277**, 10150–10155.
- 13 M. Mutter and R. Hersperger, *Angew. Chem., Int. Ed. Engl.*, 1990, **29**, 185–187.
- 14 R. A. Kammerer, D. Kostrewa, J. Zurdo, A. Detken, C. Garcia-Echeverria, J. D. Green, S. A. Mueller, B. H. Meier, F. K. Winkler, C. M. Dobson and M. O. Steinmetz, *Proc. Natl. Acad. Sci. U. S. A.*, 2004, **101**, 4435–4440.
- 15 E. Kauffmann, N. C. Darnton, R. H. Austin, C. Batt and K. Gerwert, *Proc. Natl. Acad. Sci. U. S. A.*, 2001, **98**, 6646–6649.
- 16 K. Chockalingam, M. Blenner and S. Banta, *Protein Eng., Des. Sel.*, 2007, **20**, 155–161.

- 17 H. Yokoi, T. Kinoshita and S. Zhang, *Proc. Natl. Acad. Sci. U. S. A.*, 2005, **102**, 8414–8419.
- 18 F. Gelain, A. Lomander, A. L. Vescovi and S. Zhang, *PLoS One*, 2006, **1**, e119.
- 19 Z. Luo, X. Zhao and S. Zhang, *PLoS One*, 2008, **3**, e2364.
- 20 Z. Luo, S. Wang and S. Zhang, *Biomaterials*, 2011, **32**, 2013–2020.
- 21 L. Chronopoulou, S. Lorenzoni, G. Masci, M. Dentini, A. R. Togna, G. Togna, F. Bordi and C. Palocci, *Soft Matter*, 2010, **6**, 2525–2532.
- 22 L. Chronopoulou, A. R. Togna, G. Guarguaglini, G. Masci, F. Giammaruco, G. I. Togna and C. Palocci, *Soft Matter*, 2012, **8**, 5784–5790.
- 23 A. R. Togna, V. Latina, G. Trefiletti, M. Guiso, S. Moschini and G. I. Togna, *Brain Res. Bull.*, 2013, **95**, 33–39.
- 24 H. S. Go, C. Y. Shin, S. H. Lee, S. J. Jeon, K. C. Kim, C. S. Choi and K. H. Ko, *NeuroImmunoModulation*, 2009, **16**, 365–376.
- 25 S. D. Wenker, M. E. Chamorron, D. M. Vota, M. A. Callero, D. C. Vittori and A. B. Nesse, *J. Cell. Biochem.*, 2010, **110**, 151–161.
- 26 L. Chronopoulou, M. Massimi, M. F. Giardi, C. Cametti, L. Conti Devirgiliis, M. Dentini and C. Palocci, *Colloids Surf., B*, 2013, **103**, 310–317.
- 27 M. Dentini, G. Rinaldi, A. Barbetta, D. Risica, C. Anselmi and G. Skjåk-Bræk, *Carbohydr. Polym.*, 2007, **67**, 465–473.
- 28 Z. X. Lu, K. F. Fok, B. W. Erickson and T. E. Hugli, *J. Biol. Chem.*, 1984, **259**, 7367–7370.
- 29 M. L. Waters, *Curr. Opin. Chem. Biol.*, 2002, **6**, 736–741.
- 30 A. S. Shetty, J. Zhang and J. S. Moore, *J. Am. Chem. Soc.*, 1996, **118**, 1019–1027.
- 31 C. G. Claessens and J. F. Stoddart, *J. Phys. Org. Chem.*, 1997, **10**, 254–272.
- 32 N. A. Peppas, B. V. Slaughter and M. A. Kanzelberger, *Polym. Sci.*, 2012, **9**, 385–395.